### Title
Mechanistic Modeling of Microtopographic Impacts on CO2 and CH4 Fluxes in an Alaskan Tundra Ecosystem Using the CLM-Microbe Model




### Journal
Journal of Advances in Modeling Earth Systems, 11(12)

### ISSN
1942-2466



### Authors
Wang, Yihui
Yuan, Fengming
Yuan, Fenghui
et al.



### Publication Date
2019-12-01

### DOI
10.1029/2019ms001771

Peer reviewed

JAMES | Journal of Advances in Modeling Earth Systems

RESEARCH ARTICLE
10.1029/2019MS001771

# Mechanistic Modeling of Microtopographic Impacts on $CO_2$ and $CH_4$ Fluxes in an Alaskan Tundra Ecosystem Using the CLM-Microbe Model

**Yihui Wang[1], Fengming Yuan[2], Fenghui Yuan[1,3], Baohua Gu[2], Melanie S. Hahn[4], Margaret S. Torn[5], Daniel M. Ricciuto[2], Jitendra Kumar[2], Liyuan He[1], Donatella Zona[1], David A. Lipson[1], Robert Wagner[1], Walter C. Oechel[1], Stan D. Wullschleger[2], Peter E. Thornton[2], and Xiaofeng Xu[1]**

[1]Department of Biology, San Diego State University, San Diego, CA, USA, [2]Environmental Sciences Division, Oak Ridge National Laboratory, Oak Ridge, TN, USA, [3]Institute of Applied Ecology, Chinese Academy of Sciences, Shenyang City, China, [4]Civil and Environmental Engineering, University of California, Berkeley, Berkeley, CA, USA, [5]Earth Sciences Division, Lawrence Berkeley National Laboratory, Berkeley, CA, USA

**Key Points:**
- The CLM-microbe model is able to simulate microtopographical impacts on $CO_2$ and $CH_4$ flux in the Arctic
- Substrates availability for methanogenesis is the most important factor determining $CH_4$ emission
- The strong microtopographic impacts call for a model-data integration framework to better understand and predict C flux in the Arctic

**Correspondence to:**
X. Xu,
xxu@sdsu.edu

**Citation:**
Wang, Y., Yuan, F., Yuan, F., Gu, B., Hahn, M. S., Torn, M. S., et al (2019). Mechanistic Modeling of Microtopographic Impacts on $CO_2$ and $CH_4$ Fluxes in an Alaskan Tundra Ecosystem Using the CLM-Microbe Model. *Journal of Advances in Modeling Earth Systems*, *11*. https://doi.org/10.1029/2019MS001771

Received 2 JUN 2019
Accepted 11 OCT 2019
Accepted article online 22 NOV 2019



**Abstract** Spatial heterogeneities in soil hydrology have been confirmed as a key control on $CO_2$ and $CH_4$ fluxes in the Arctic tundra ecosystem. In this study, we applied a mechanistic ecosystem model, CLM-Microbe, to examine the microtopographic impacts on $CO_2$ and $CH_4$ fluxes across seven landscape types in Utqiaġvik, Alaska: trough, low-centered polygon (LCP) center, LCP transition, LCP rim, high-centered polygon (HCP) center, HCP transition, and HCP rim. We first validated the CLM-Microbe model against static-chamber measured $CO_2$ and $CH_4$ fluxes in 2013 for three landscape types: trough, LCP center, and LCP rim. Model application showed that low-elevation and thus wetter landscape types (i.e., trough, transitions, and LCP center) had larger $CH_4$ emissions rates with greater seasonal variations than high-elevation and drier landscape types (rims and HCP center). Sensitivity analysis indicated that substrate availability for methanogenesis (acetate, $CO_2 + H_2$) is the most important factor determining $CH_4$ emission, and vegetation physiological properties largely affect the net ecosystem carbon exchange and ecosystem respiration in Arctic tundra ecosystems. Modeled $CH_4$ emissions for different microtopographic features were upscaled to the eddy covariance (EC) domain with an area-weighted approach before validation against EC-measured $CH_4$ fluxes. The model underestimated the EC-measured $CH_4$ flux by 20% and 25% at daily and hourly time steps, suggesting the importance of the time step in reporting $CH_4$ flux. The strong microtopographic impacts on $CO_2$ and $CH_4$ fluxes call for a model-data integration framework for better understanding and predicting carbon flux in the highly heterogeneous Arctic landscape.

## 1. Introduction

Spatial heterogeneity in land surface properties has been shown to be a key source of large variabilities and uncertainties in $CO_2$ and $CH_4$ fluxes in the Arctic (Bridgham et al., 2013; Davidson et al., 2016; Sturtevant & Oechel, 2013; Xu et al., 2014; Zona et al., 2011). Polygonal ground patterns create a complex mosaic of microtopographic features with poorly drained low-centered polygons (LCPs) surrounded by high rims and well-drained high-centered polygons (HCPs) surrounded by low trough as results of the annual freeze–thaw cycles across the northern Alaskan coastal plain (Hinkel et al., 2005; Throckmorton et al., 2015; Zona et al., 2011). Microtopography strongly affects soil water content and active layer depth (Atchley et al., 2016; Grant, Mekonnen, Riley, Arora, & Torn, 2017a; Grant, Mekonnen, Riley, Wainwright, et al., 2017b; Lu & Zhuang, 2012), soil temperature and thermal conductivity (Abolt et al., 2018; Kumar et al., 2016), soil pH and $O_2$ availability (Lipson et al., 2012; Zona et al., 2011), soil chemistry (Lipson et al., 2013; Newman et al., 2015; Semenchuk et al., 2015), vegetation types and canopy height (Davidson et al., 2016; von Fischer et al., 2010), and microbial community structure (Tas et al., 2018; Wagner et al., 2017). Therefore, the large spatial heterogeneities in microtopographic features are critically important for modeling and predicting the ecosystem carbon (C) exchange in Arctic tundra ecosystems.

Previous studies have found that Arctic tundra ecosystems have shifted from net $CO_2$ sinks to sources (Belshe et al., 2013; Oechel et al., 1993); whether they behave as sinks or sources of atmospheric $CH_4$

largely depends on local microtopography (Jørgensen et al., 2014; Nauta et al., 2015; Oh et al., 2016; Tan et al., 2015). Minor changes in surface elevation might shift Arctic soils from sinks to sources of atmospheric $CH_4$ (Olivas et al., 2010; Zona et al., 2011). $CH_4$ is produced in the poorly drained low-elevation ground with anoxic conditions, whereas atmospheric $CH_4$ can be oxidized in well-drained high-elevation ground (Atchley et al., 2016; Grant, Mekonnen, Riley, Arora, & Torn, 2017a; Lipson et al., 2012; von Fischer et al., 2010; Zona et al., 2011). Microtopography also affects the $CO_2$ flux by altering the soil water content and $O_2$ concentration (Olivas et al., 2010). In addition, soil hydrological conditions affect vegetation growth and substrate availability, further influencing ecosystem C input and microbial community structure and altering the transport and production of $CH_4$, root respiration, and microbial respiration (Davidson et al., 2016; von Fischer et al., 2010; Wagner et al., 2017). Thus, accurate quantification of the strength of C sinks or sources requires explicit consideration of the microtopographic effects on C cycling in Arctic tundra ecosystems (Ebrahimi & Or, 2017).

To more accurately capture the fine-scale variations in $CH_4$ and $CO_2$ fluxes in Arctic tundra, microtopographic effects need to be considered by ecosystem models as microbial functions such as fermentation, C mineralization, methanogenesis, and methanotrophy dramatically differ between wet and dry polygons (Tas et al., 2018). A number of mechanistic $CH_4$ models have incorporated the mechanisms of $CH_4$ production, consumption, and transport pathways (Xu et al., 2016), such as the *ecosys* model (Grant, Mekonnen, Riley, Arora, & Torn, 2017a), CLM-Microbe (Xu et al., 2015), CLM4Me (Riley et al., 2011), LPJ-WHyMe (Wania et al., 2010), and NEST-DNDC (Zhang et al., 2012). However, few $CH_4$ models explicitly simulate microtopography and are capable of investigating the microtopographic impacts on $CO_2$ and $CH_4$ fluxes in Arctic tundra (Grant, Mekonnen, Riley, Arora, & Torn, 2017a; Kaiser et al., 2017). For example, the *ecosys* model indicates that microtopography determines $CO_2$ and $CH_4$ emissions by regulating soil water content, active layer depth, and $O_2$ availability (Grant, Mekonnen, Riley, Arora, & Torn, 2017a). The CLM-Microbe model simulates fine-scale thermal and hydrological dynamics and microbial mechanisms for $CH_4$ production and oxidation (Xu et al., 2015), which allows investigation of Arctic $CO_2$ and $CH_4$ fluxes across multiple scales from a microbial perspective.

In this study, we used the CLM-Microbe model to simulate the microtopographic effects on $CO_2$ and $CH_4$ flux. We aimed to address three questions: (1) How do different microtopographic types affect $CO_2$ and $CH_4$ fluxes in Arctic tundra ecosystems? (2) Which processes are more important in controlling $CO_2$ and $CH_4$ fluxes among the microtopographic types? (3) How do annual estimates of $CO_2$ and $CH_4$ fluxes differ under the microtopographic impacts in the Arctic? The field observational data from the U.S. Department of Energy's Office of Science Next Generation Ecosystem Experiments (NGEE)-Arctic project were integrated with the CLM-Microbe model to understand microtopographic impacts on land surface $CO_2$ and $CH_4$ fluxes in an Arctic tundra landscape.

## 2. Methodology

### 2.1. Site Information and Experimental Data

#### 2.1.1. Site Description

Our study area is located within the Barrow Environmental Observatory (BEO), ~6 km east of Utqiaġvik (formerly Barrow), Alaska (71.3°N, 156.5°W), operated by the NGEE-Arctic project (https://ngee-arctic.ornl.gov/). It has a polar maritime climate with mean annual air temperature of −12.0 °C in winter and 3.3 °C in summer (June–August), and with mean annual precipitation of 173 mm and the majority of precipitation falling during summer months (Liljedahl et al., 2011). Snowmelt usually ends in early to mid-June and the wind direction is predominantly from east to west throughout the year (Wainwright et al., 2017). The dominant plants are mosses (*Dicranum elongatum*, *Sphagnum*), lichens, and vascular plants (such as *Carex aquatilis*); plant distribution is governed by surface moisture variability (Zona et al., 2011).

The landscapes are highly heterogeneous with polygonal landscape patterns. The NGEE-Arctic project established four 100 m × 100 m intensively sampled areas within the BEO (Langford et al., 2016). The sampled areas are dominated by the LCPs and HCPs with internal features of center, rim, transition, and trough (Figure 1a). Accordingly, seven landscape types were classified within the study area: trough (35.0% of total area), LCP center (6.9%), LCP rim (12.2%), LCP transition (14.3%), HCP center (13.2%),

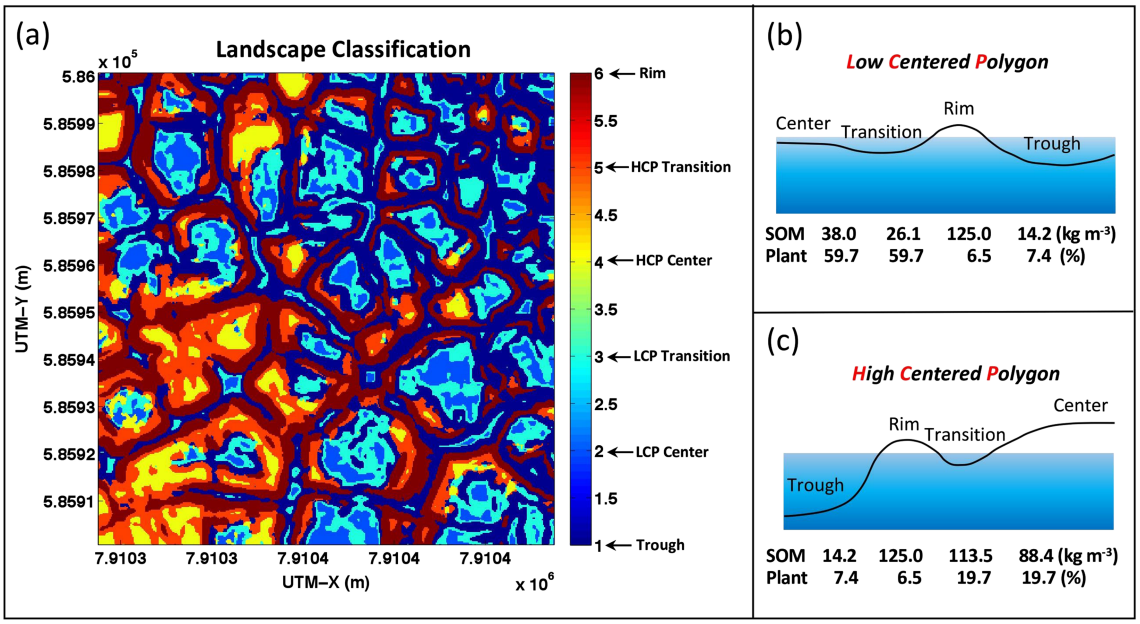


**Figure 1.** (a) The landscape classification map for area C (100 m × 100 m). Red indicates high surface elevation and blue indicates low surface elevation. Values on the legend are indexes used to identify different landscape types. Diagrams depict the landscape types for (b) low-centered polygon and (c) high-centered polygon with internal polygonal feature: center, rim, transition, and trough (Yuan et al., 2017).

HCP rim (12.2%), and HCP transition (6.2%). Soil organic matter density and plant cover used in model simulations for each landscape type are shown in Figure 1.

#### 2.1.2. Data Availability Statement

The $CH_4$ and $CO_2$ fluxes were monitored using the static chamber approach on several dates during June–September 2012 and 2013 (Torn, 2016). Transparent and opaque surface chambers were placed within the study area in the trough, LCP center, and LCP rim. The $CO_2$ fluxes from the transparent chambers were considered to be the net ecosystem exchange of $CO_2$ (NEE), and those from the opaque chambers were considered the ecosystem respiration (ER). NEE (i.e., ER − GPP) is negative when $CO_2$ uptake via photosynthesis is greater than $CO_2$ release from ER. The concentrations of soil dissolved organic carbon (DOC), $CH_4$, and $CO_2$ were measured for the trough, LCP center, and LCP rim in 2013–2014 (Herndon et al., 2015a; Herndon et al., 2015). An eddy covariance (EC) tower was installed in the center of the study area to measure $CO_2$ and $CH_4$ fluxes in 2012; those data are available from the NGEE Arctic project website (Raz-Yaseef et al., 2013). It is noted that this data set has been updated to 2012–2016 although we used the previous data set for 2012–2013. Daily and hourly fluxes of $CH_4$ and $CO_2$ were calculated based on the half-hourly EC data. Detailed information about the measurement protocols is posted in the NGEE Arctic archives (http://ngee-arctic.ornl.gov/).

### 2.2. Modeling Experiment

#### 2.2.1. Model Description and Driving Data

The CLM-Microbe model branches from the framework of default CLM 4.5 by developing a new representation of $CH_4$ production and consumption (Xu et al., 2015), in association with the decomposition subroutines in CLM4.5 (Koven et al., 2013; Thornton et al., 2007; Thornton & Rosenbloom, 2005). It incorporates new mechanisms of DOC fermentation, hydrogenotrophic methanogenesis, acetoclastic methanogenesis, aerobic methanotrophy, anaerobic methanotrophy, and $H_2$ production based on known processes (Thauer et al., 1989; Thauer et al., 2008) and adopted from previous modeling studies (Grant, 1998; Kettunen, 2003; Riley et al., 2011; Segers & Kengen, 1998; Tian et al., 2010; Walter & Heimann, 2000; Xu et al., 2010; Zhuang et al., 2004). Detailed mathematical expressions for $CH_4$ production and consumption processes were organized in Xu et al. (2015). The code for the CLM-Microbe model is archived at this site (https://github.com/email-clm/clm-microbe). The model version used in this study was checked out from GitHub on 18 June 2018.

**Table 1**
*Key Parameters for Model Parameterization*

| Types | *KAce* | *AceProdACmax* | *k_dom* | *k_bacteria* | *k_fungi* | *fatm_f* | *Grperc* |
|---|---|---|---|---|---|---|---|
| Default value | 16 | 2.4e-06 | 0.007 | 0.22 | 0.22 | 0.20 | 0.1652 |
| Trough | 12 | 6.4e-06 | 0.014 | 0.05 | 0.05 | 0.15 | 0.0052 |
| LCP center | 12 | 1.8e-06 | 0.007 | 0.01 | 0.01 | 0.12 | 0.0052 |
| LCP rim | 12 | 1.2e-06 | 0.007 | 0.01 | 0.01 | 0.05 | 0.0052 |
| LCP transition | 16 | 6.4e-06 | 0.007 | 0.22 | 0.22 | 0.20 | 0.0052 |
| HCP transition | 16 | 6.4e-06 | 0.007 | 0.22 | 0.22 | 0.20 | 0.0052 |
| HCP center | 16 | 2.4e-06 | 0.007 | 0.22 | 0.22 | 0.20 | 0.0052 |
| HCP rim | 16 | 2.4e-06 | 0.007 | 0.22 | 0.22 | 0.20 | 0.0052 |

*Note*. LCP = low-centered polygon; HCP = high-centered polygon.

In a previous study, the $CH_4$ module in the CLM-Microbe model was validated for simulating the dynamics of $CO_2$ and $CH_4$ emissions from incubation experiments on Arctic soils with invariant soil temperature and soil water content (Xu et al., 2015). In this study, we focused on the fully incorporated CLM-Microbe model, created separate model runs for each landscape type, and modified the soil hydrological setup according to landscapes' unique soil conditions. Three soil hydrological parameters, largely affected by microtopography, were selected: soil water content (*h2osoi_vol*), surface runoff (*qflx_surf*), and the inundated fraction (*finundated*). Because the low-elevation polygonal features, such as trough, LCP center, LCP transition, and HCP transition are poorly drained and oversaturated in summer, the parameters for soil water content were changed to a maximum of 1.0, and those for the inundated fraction and surface runoff were changed to 0.99 and 0, respectively. In contrast, the high-elevation features, such as LCP rim, HCP rim, and HCP center, are well-drained in summer. For these features, the parameters for soil water content were set at a maximum of 0.3, which is the baseline allowing the gas transport in soil profiles due to model structures; and those for surface runoff and inundated fraction were set in the default processes with dynamic changes.

The model driving data included meteorological, plant, and soil data. The meteorological data included shortwave and longwave radiation, air temperature, relative humidity, wind speed, and precipitation from 1 January 1991 to 31 December 2014, derived by *Xu and Yuan* (2016) from the Utqiaġvik, AK, station of NOAA/Earth System Laboratory, Global Monitoring Division (http://www.esrl. noaa.gov/gmd/obop/brw/ ). The data set is gap-filled and at a half-hour time step. The observed plant and soil data for each landscape type—including the composition of plant functional types, plant cover, and soil organic carbon density—were supplied by the NGEE Arctic project.

### 2.2.2. Model Implementation

To identify the role of microbial functions in $CH_4$ dynamics, we set up model simulations using the default CLM4.5 and the CLM-Microbe models separately for each landscape type. The model implementation was carried out in three stages. First, the accelerated model spin-up was set up for 2,000 years to allow the system to accumulate C. Then a final spin-up for 50 years allowed the modeled system to reach a relatively steady state. After the final spin-up, the transient model simulation was set up to cover the period of 1850–2014.

For the default CLM4.5 model simulations, the parameters were set to be the default values for each landscape type. For the CLM-Microbe model simulations, the model parameterization was initialized with the default parameters in Xu et al. (2015); it was performed within their ranges to determine the optimal values of parameters in the microbial module for simulating the observational $CO_2$ and $CH_4$ fluxes for each landscape type. For the trough, LCP center, and LCP rim, the observed $CO_2$ and $CH_4$ fluxes in 2012 were used for model parameterization, and the fluxes in 2013 were used for model validation. Based on the current knowledge of mechanisms of $CO_2$ and $CH_4$ cycling, we primarily focused on the parameters for decomposition and substrate availability for methanogenesis (e.g., *k_bacteria, k_fungi, KAce*, and *AceProdACmax*) for the $CH_4$ cycling. For $CO_2$ cycling, we focused on the parameters for plant growth respiration (*grperc*), maintenance respiration (*br_mr*), and C allocation within biogeochemical cascade (e.g., *fatm_f*). According to the values of parameters reported in the previous studies, the parameters were calibrated empirically in the model parameterization (Table 1). Because of the lack of the observational data, most of the parameters for LCP transition, HCP center, HCP rim, and HCP

**Table 2**
*Key Parameters for Uncertainty Analysis and Sensitivity Analysis.*

| Parameter | Ecological meaning |
|---|---|
| *KAce* | Half-saturation coefficient of available carbon mineralization |
| *ACminQ10* | Temperature sensitivity of available carbon mineralization |
| *AceProdACmax* | Maximum rate of acetate production from available carbon |
| *H2ProdAcemax* | Maximum rate of $H_2$ production from available acetate |
| *KH2ProdAce* | Half-saturation coefficient of conversion of $H_2$ and $CO_2$ to acetate |
| *KCO2ProdAce* | Assuming it is half of that for $H_2$ based on stoichiometry theory |
| *KCO2ProdCH4* | Half coefficient of $CO_2$ for methane production from $H_2$ |
| *GrowRAceMethanogens* | Growth rate of acetoclastic methanogens |
| *YAceMethanogens* | Growth efficiency of acetoclastic methanogens |
| *k_dom* | Decomposition rate constant dissolved organic matter |
| *k_bacteria* | Decomposition rate constant biomass of bacteria |
| *k_fungi* | Decomposition rate constant biomass of fungi |
| *flnr* | Fraction of leaf N in the Rubisco enzyme |
| *grperc* | Growth respiration parameter |
| *br_mr* | Base rate of maintenance respiration |

transition, were set as the default values; and some parameters were modified according to the setup for the trough, LCP center, and LCP rim (Table 1). The transient simulations of 1850–2014 produced output at both daily and hourly time steps. Simple linear regression was conducted to evaluate the modeled $CO_2$ and $CH_4$ fluxes compared with measured fluxes. The error statistics were used to distinguish the difference between the modeled and measured fluxes on the platform of *R* Studio platform (version 1.1.456), such as the coefficient of determination ($R^2$).

### 2.2.3. Uncertainty Analysis

The uncertainties of the $CO_2$ and $CH_4$ fluxes for each landscape type were quantified using the Markov Chain Monte Carlo method based on Bayesian statistics (Gilks et al., 1998) and were determined by a large ensemble of model simulations with different parameter settings. In this study, a total of 100 model simulations with different settings of 15 key parameters were set up for each landscape type, separately. These 15 key parameters determine the decomposition of organic carbon, methanogenesis, microbial growth, and plant photosynthesis and respiration and therefore control the $CO_2$ and $CH_4$ fluxes (Table 2). They varied within a range of 30% of their optimal values (Xu et al., 2015). Model simulations were conducted from the transient simulation to cover 1850–2014 at a daily time step.

### 2.2.4. Area-Weighted Upscaling

The modeled $CO_2$ and $CH_4$ fluxes in 2013 for each landscape type were further used for upscaling to the EC tower domain based on an area-weighted average approach. Because of the limitation of the landscape classification data, the EC domain was confined to an area of 100 m × 100 m. The area-weighted average approach includes information for landscape heterogeneity in the upscaling process. The upscaled flux was calculated by the following equation:

$$F = \sum_{i=1}^{n} f_i \times \mathrm{area}_i \quad (1)$$

where $F$ is the upscaled plot flux for the EC domain, $f_i$ is the plot-level $CH_4$ or $CO_2$ fluxes for a given landscape type for a given time period, $area_i$ is the fraction of each major landscape type within the EC domain (Davidson et al., 2016). In addition, the average fluxes were calculated based on the $CH_4$ and $CO_2$ fluxes from the seven landscape types for comparison with the upscaled fluxes.

### 2.2.5. Sensitivity Analysis

To identify the most important process and the most sensitive parameters for $CH_4$ and $CO_2$ dynamics in Arctic tundra, a global sensitivity analysis was conducted for each microtopographic type. It focused on the 15 parameters related to plant and microbial processes that were used in the uncertainty analysis (Table 2). For each parameter, we set up model simulations with +20% and − 20% changes and investigated the responses of the modeled $CH_4$ and $CO_2$ fluxes in 2013. The index *S*, comparing the change in the model output relative to the model response for a nominal set of parameters, was calculated based on the flowing equation (Xu et al., 2015):

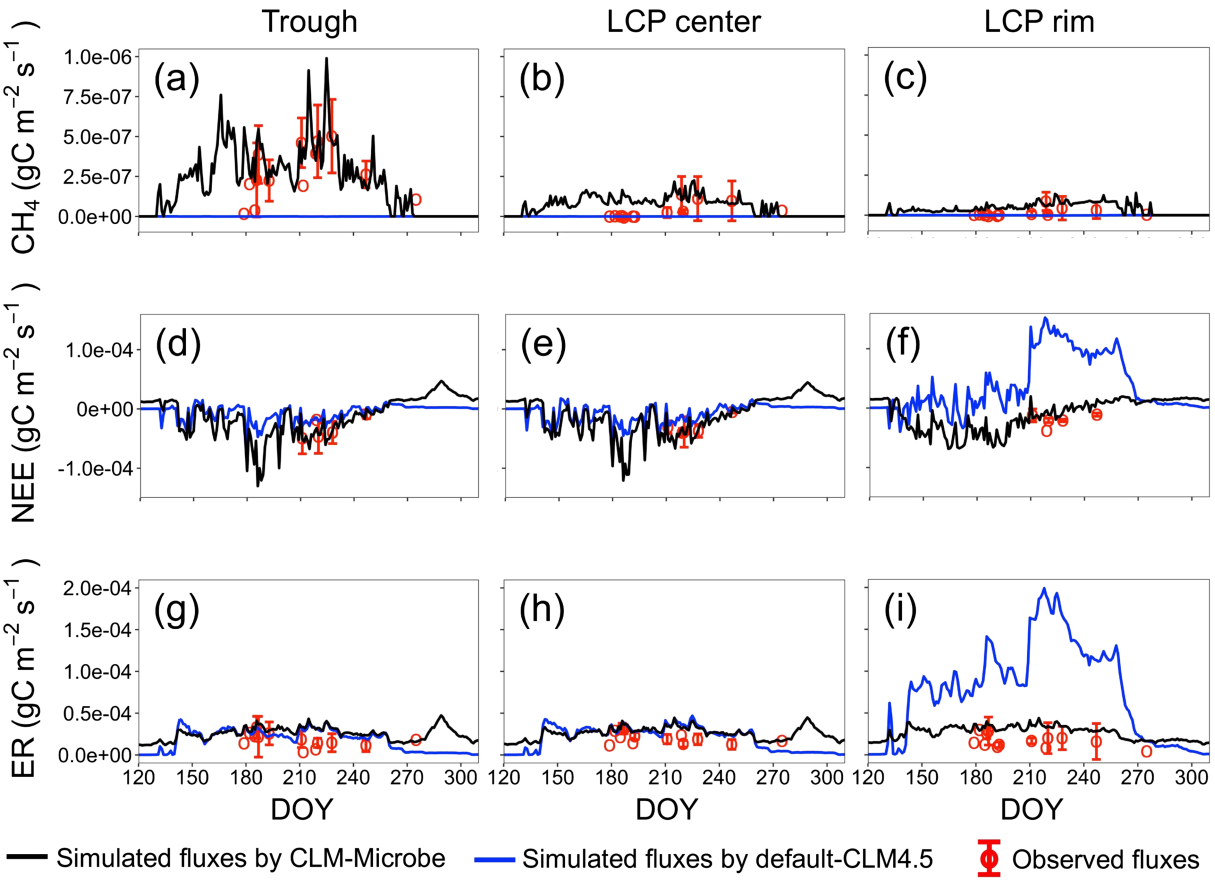


**Figure 2.** Simulated (a–c) $CH_4$ fluxes, (d–f) net ecosystem carbon exchange (NEE), and (g–i) ecosystem respiration (ER) for trough, low-centered polygon (LCP) center, and LCP rim compared with observational fluxes from static chambers (red circles with error bars) from May to September 2013 (Torn, 2016). The black lines indicate the modeled fluxes simulated by the CLM-microbe model, and the blue lines indicate the default fluxes simulated by the default CLM4.5. The blue lines are not smooth for $CH_4$ fluxes; the fluxes are negative and are too small to show.

$$S = \frac{(Ra - Rn)/Rn}{(Pa - Pn)/Pn} \tag{2}$$

where $S$ is the ratio of the standardized change in model response to the standardized change in parameter values. $R_a$ and $R_n$ are model responses for altered and nominal parameters, respectively, and $P_a$ and $P_n$ are the altered and nominal parameters, respectively. $S$ is negative if the direction of model response opposes the direction of parameter change (Xu et al., 2015).

## 3. Results

### 3.1. Model-Simulated $CH_4$ and $CO_2$ Fluxes

The CLM-Microbe model was more accurate than the default CLM4.5 in simulating the $CH_4$ and $CO_2$ fluxes during the summer of 2013 (Figure 2). The dynamics of $CH_4$ was captured well by the CLM-Microbe model for the trough, LCP center, and LCP rim, but those sites were simulated as a small $CH_4$ sink in summer by the default CLM4.5 (Figures 2a–2c and Table 3). NEE and ER were used to represent the dynamics of $CO_2$ flux. In the summer months, NEE and ER had the similar patterns for the trough and LCP center but showed significant differences for LCP rim in the default CLM4.5 and CLM-Microbe models (Figures 2d–2i). For the trough and LCP center, the CLM-Microbe model simulated the NEE well, whereas the default model underestimated it by 47–50%; however, both of them overestimated the ER by 28–47% (Figure 3 and Table 3). The variations of NEE and ER were not captured by either the default or the CLM-Microbe models for LCP rim, but the CLM-microbe model performed slightly better than the default model (Figure 3 and Table 3).

**Table 3**
*Linear Regression Analysis for $CH_4$ flux, Net Ecosystem Carbon Exchange (NEE), and Ecosystem Respiration (ER) for Model Validation of the CLM-Microbe Model and the Default CLM4.5*

| Site | Variable | Estimate | Std. error | *P* value | $R^2$ |
|---|---|---|---|---|---|
| Trough | Modeled CH4 | 1.0626 | 0.1827 | 0.0001* | 0.7381 |
| | Default CH4 | −0.0027 | 0.0003 | 0.0000* | 0.8388 |
| LCP center | Modeled CH4 | 1.0167 | 0.4683 | 0.0507 | 0.2820 |
| | Default CH4 | −0.0090 | 0.0038 | 0.0341 | 0.3226 |
| LCP rim | Modeled CH4 | 1.0925 | 0.4363 | 0.0277 | 0.3432 |
| | Default CH4 | −0.0309 | 0.0093 | 0.0060* | 0.4802 |
| Trough | Modeled NEE | 0.9961 | 0.1057 | 0.0007* | 0.9569 |
| | Default NEE | 0.4957 | 0.0650 | 0.0016* | 0.9356 |
| LCP center | Modeled NEE | 1.0572 | 0.1565 | 0.0025* | 0.9194 |
| | Default NEE | 0.4711 | 0.1216 | 0.0179 | 0.7895 |
| LCP rim | Modeled NEE | 0.2160 | 0.2339 | 0.4080 | 0.1757 |
| | Default NEE | −5.1333 | 0.7907 | 0.0029* | 0.9133 |
| Trough | Modeled ER | 1.4729 | 0.1913 | 0.0000* | 0.8316 |
| | Default ER | 1.2800 | 0.2028 | 0.0000* | 0.7685 |
| LCP center | Modeled ER | 1.3922 | 0.1195 | 0.0000* | 0.9188 |
| | Default ER | 1.4301 | 0.1456 | 0.0000* | 0.8893 |
| LCP rim | Modeled ER | 1.6449 | 0.1753 | 0.0000* | 0.8800 |
| | Default ER | 6.4249 | 0.9320 | 0.0000* | 0.7984 |

*Note*. LCP = low-centered polygon.
*The significant level < 0.01.

For the simulations of the CLM-Microbe model, larger $CH_4$ fluxes with greater variations were observed for the trough than that for the LCP center and LCP rim (Figures 2a–2c). Additionally, modeled $CH_4$ fluxes were more consistent with the observational fluxes for the trough ($R^2$ = 0.7381, $p$ = 0.0001) than for the LCP center ($R^2$ = 0.2820, $p$ = 0.0507) and LCP rim ($R^2$ = 0.3432, $p$ = 0.0277; Table 3). For the dynamics of $CO_2$ fluxes, similar patterns of NEE and ER were simulated for the trough and LCP center (Figures 2d and 2e). Modeled NEE was highly consistent with the observed data for the trough ($R^2$ = 0.9569, $p$ = 0.0007) and LCP center ($R^2$ = 0.9194, $p$ = 0.0025); whereas ER was overestimated by 47.3% for the trough ($R^2$ = 0.8316, $p$ < 0.0001) and 39.2% for the LCP center ($R^2$ = 0.9188, $p$ < 0.0001; Table 3). Compared with the trough and LCP center, a slightly higher NEE (lower $CO_2$ uptake) was modeled for the LCP rim and it was underestimated by 78.4% ($R^2$ = 0.4080, $p$ = 0.1757; Table 3). However, ER for the LCP rim was overestimated by 64.5% ($R^2$ = 0.88, $p$ < 0.0001; Table 3).

### 3.2. Variability and Seasonality of $CH_4$ and $CO_2$ Fluxes Across the Arctic Landscape Types

Modeled $CH_4$ and $CO_2$ fluxes exhibited large variabilities among all seven landscape types. In the summer months, high $CH_4$ emissions were generally simulated, associated with low NEE (i.e., high $CO_2$ uptake) and high

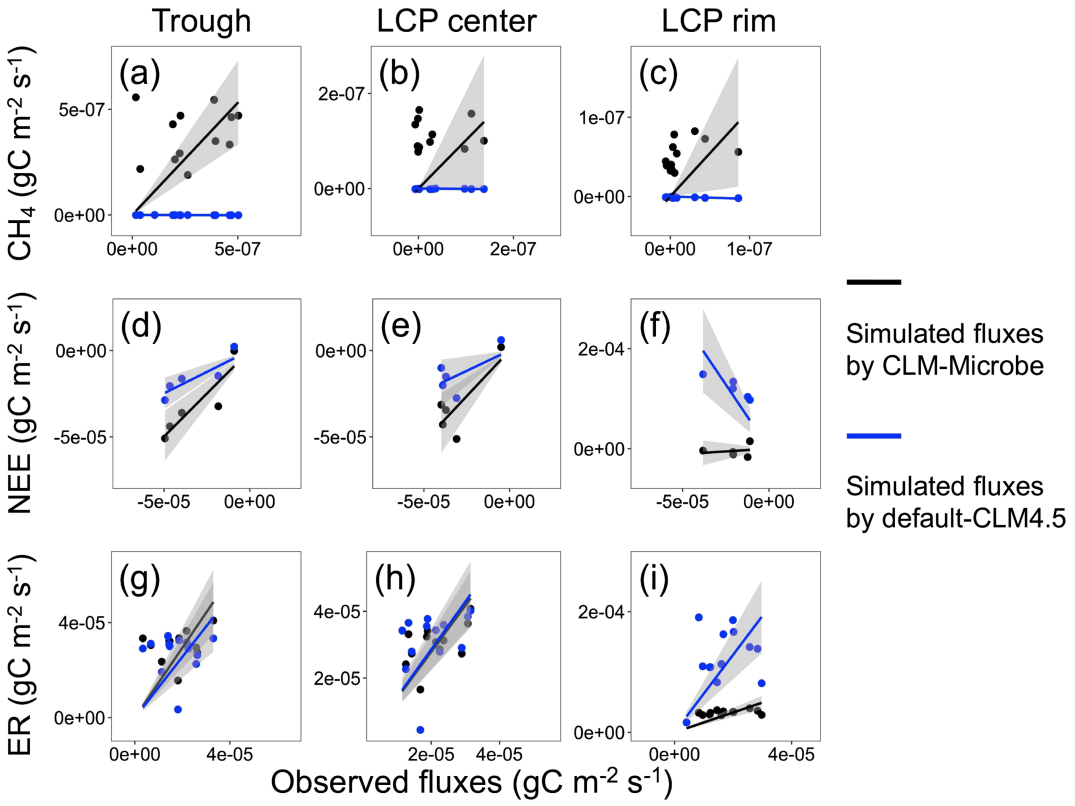


**Figure 3.** Scatter plots of observed versus simulated (a–c) $CH_4$ fluxes, (d–f) net ecosystem carbon exchange (NEE), and (g–i) ecosystem respiration (ER) for trough, low-centered polygon (LCP) center, and LCP rim, with linear lines of best fit (no interception) and 95% confidence interval for regression line shaded gray. The black lines and points indicate the relationship between observed fluxes and modeled fluxes simulated by the CLM-microbe model. The blue lines and points indicate the relationship between observed fluxes and the default fluxes simulated by the default CLM4.5.

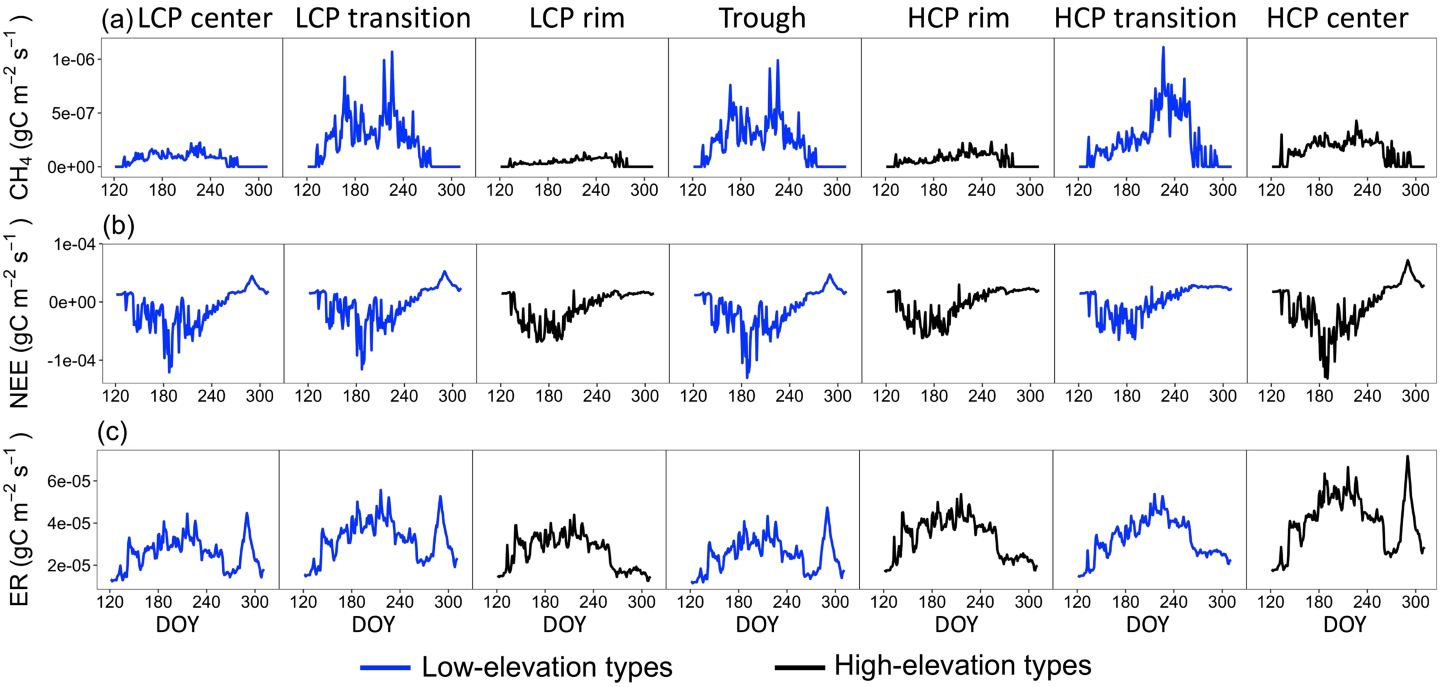


**Figure 4.** Modeled (a) $CH_4$ fluxes, (b) net ecosystem carbon exchange (NEE), and (c) ecosystem respiration (ER) for all seven landscapes types in 2013. The black lines indicate the high-elevation types, and blue lines indicate the low-elevation types. LCP = low-centered polygon; HCP = high-centered polygon.

ER for all the landscape types (Figure 4). Low-elevation landscape types, such as trough, LCP transition, and HCP transition, had higher $CH_4$ emissions with greater variation compared with high-elevation types, such as LCP rim, HCP rim, and HCP center (Figure 4a). However, low-elevation types, including trough, LCP transition, and LCP center showed lower NEE (i.e., higher $CO_2$ uptake) than high-elevation types, including LCP rim and HCP rim (Figure 4b). ER was roughly higher in the HCP center and lower in the trough and LCP center in the summer months (Figure 4c).

Larger seasonal variations of $CH_4$ dynamics were modeled in low-elevation landscape types (e.g., trough and transitions) than high-elevation types (e.g., rim; Figure 4a). In the early spring, most of the landscape types showed a burst release of $CH_4$ flux, corresponding to the early Spring thaw. During the growing seasons, the lower ground of the trough and LCP transition had similar seasonality of $CH_4$ and $CO_2$ fluxes, with the highest $CH_4$ emission and highest $CO_2$ uptake (Figure 4). The higher ground of rims tended to have smaller variations of $CH_4$ and NEE fluxes (Figure 4). A sudden rise was simulated in NEE for the trough, LCP transition, LCP center and HCP center, during the late growing seasons; a similar rise simultaneously was simulated in ER (Figure 4).

### 3.3. Annual Estimates of $CH_4$ and $CO_2$ Fluxes Across the Landscape Types

Annual $CH_4$ fluxes were estimated for all landscape types, resulting in a range of 0.66 to 3.97 g $Cm^{-2}$ (Table 4). The HCP transition, as the largest $CH_4$ source, has released 5.06 times more annual $CH_4$ fluxes more than the smallest $CH_4$ sources (i.e., LCP rim). Low-elevation types, including trough and transition, contributed a larger proportion of $CH_4$ emissions than high-elevation types in Arctic tundra ecosystems. Based on the areal fractions, the HCPs and LCPs were estimated to have comparable annual $CH_4$ fluxes of 2.12 and 2.19 g C $m^{-2}$ $year^{-1}$, respectively, both of which were smaller than the annual $CH_4$ fluxes of 3.63 g C $m^{-2}$ $year^{-1}$ from the trough (Table 4).

The landscape types were found to be net sources of $CO_2$, except for the trough, in which 21.08 g C·$m^{-2}$·$year^{-1}$ of $CO_2$ was sequestered (Table 4). Large variations existed in the annual NEE, which ranged from −21.08 to 248.22 g C·$m^{-2}$·$year^{-1}$ (Table 4). The HCP transition was the largest $CO_2$ source to the atmosphere among the landscape types. All the landscape types had comparable ERs—

**Table 4**
*Annual Estimates of $CH_4$ Flux, Net Ecosystem Carbon Exchange (NEE) and Ecosystem Respiration (ER) (g C·m$^{-2}$·year$^{-1}$) With the Uncertainties for All Seven Landscape Types, the Average and the Area-Weighted Average (AWA) for the EC Domain Based on Modeled Daily Fluxes in 2013*

| Type | $CH_4$ flux | NEE | ER |
|---|---|---|---|
| Trough | 3.632 (3.403–3.887) | −21.083 (−26.187 to −16.546) | 582.715 (581.149–584.086) |
| LCPcenter | 1.145 (1.117–1.175) | 3.056 (−8.265–10.780) | 598.520 (586.288–606.655) |
| LCPrim | 0.656 (0.575–0.678) | 19.579 (11.464–22.378) | 617.660 (613.992–625.929) |
| LCPtransition | 3.835 (3.714–3.971) | 160.928 (157.811–165.165) | 754.986 (752.519–755.857) |
| HCPcenter | 2.384 (2.296–2.461) | 137.940 (130.614–145.714) | 927.981 (923.071–930.792) |
| HCPrim | 1.075 (1.029–1.130) | 180.277 (177.880–181.020) | 776.309 (774.682–782.879) |
| HCPtransition | 3.974 (3.839–4.121) | 248.219 (246.895–251.471) | 759.463 (758.276–761.238) |
| Average | 2.386 | 104.131 | 716.805 |
| AWA | 2.671 | 73.825 | 692.855 |

*Note.* LCP = low-centered polygon; HCP = high-centered polygon.

ranging from 582.72 to 776.31 g C·m$^{-2}$·year$^{-1}$—except the HCP center, which exhibited the greatest ER of 927.98 g C·m$^{-2}$·year$^{-1}$. The trough, LCP center, and LCP rim with smaller NEE estimates were also estimated to have smallest ER budget.

### 3.4. Upscaling $CH_4$ and $CO_2$ Fluxes to the EC Domain

Modeled $CH_4$ and $CO_2$ fluxes were upscaled to the EC domain based on the area fraction of each landscape type. High consistency was shown between the upscaled fluxes and EC measurements (Figures 5 and 6). The regression analysis showed that more accurate simulations of $CH_4$ and NEE fluxes for the EC domain were obtained at daily time steps than at hourly time steps (Figure 6). $CH_4$ fluxes were underestimated at daily ($R^2 = 0.7931$, $p < 0.0001$) and hourly ($R^2 = 0.6135$, $p < 0.0001$) time steps by 20.08% and 24.95%, respectively. NEE was underestimated at the daily time steps by 21.44% ($R^2 = 0.2843$, $p < 0.0001$), but was overestimated at the hourly time steps by 30.01% ($R^2 = 0.3464$, $p < 0.0001$; Table 5).

Annual $CH_4$ and $CO_2$ fluxes were estimated for the EC domain using the arithmetic average and area-weighted average approaches. When the proportions of different landscape types were not considered, the annual $CH_4$ flux was underestimated at 2.39 g C·m$^{-2}$·year$^{-1}$, compared with an annual estimate of

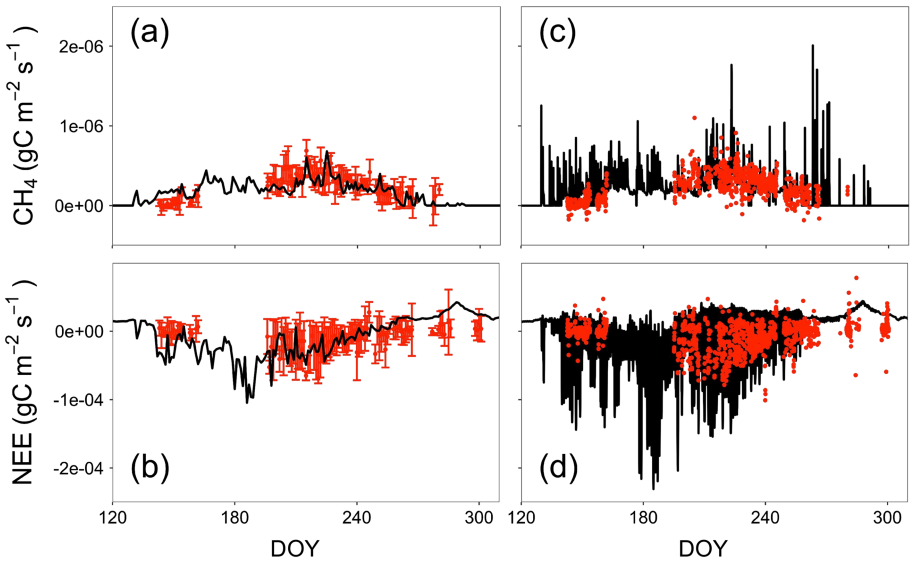


**Figure 5.** Upscaled (a, b) $CH_4$ fluxes and (c, d) net ecosystem carbon exchange (NEE) comparing with measured fluxes from an eddy covariance tower centered in the study area at the daily (a, c) and hourly (b, d) time steps in 2013. Black lines indicate the gas fluxes and red points with/without error bars indicate measured fluxes. DOY = day of year.

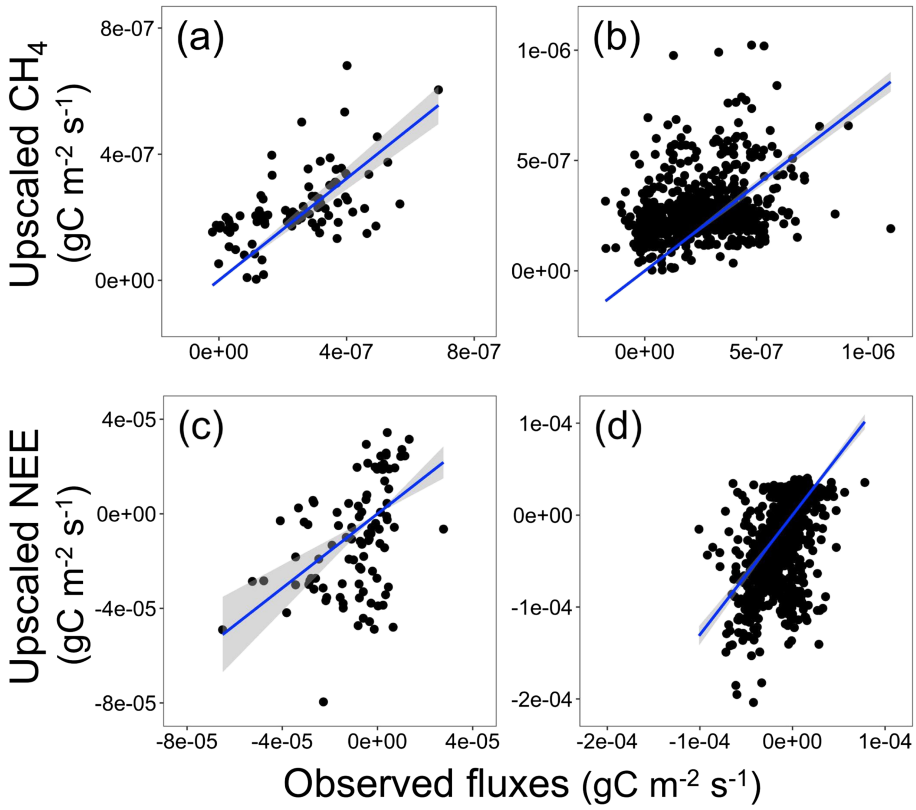


**Figure 6.** Scatter plots of measured versus upscaled $CH_4$ (a, b) and net ecosystem carbon exchange (NEE) (c, d) at daily (a, c) and hourly (b, d) time steps for the eddy covariance domain of the study area in 2013, with linear lines of best fit (no interception) and 95% confidence interval for regression line shaded gray.

2.67 g C·m$^{-2}$·year$^{-1}$ based on the areal fractions. However, NEE and ER were overestimated at 104.13 g C·m$^{-2}$·year$^{-1}$ and 716.81 g C·m$^{-2}$·year$^{-1}$, respectively, compared with the annual estimates of 73.83 g C·m$^{-2}$·year$^{-1}$ and 692.86 g C·m$^{-2}$·year$^{-1}$ for NEE and ER, respectively, that considered the heterogeneity of landscapes (Table 4).

### 3.5. Sensitivity Analysis

$CH_4$ and $CO_2$ fluxes were sensitive to a portion of the key parameters that are related to available carbon mineralization, $CH_4$ production, growth of methanogens, decomposition, photosynthesis, plant growth respiration, and maintenance respiration. Specifically, the $CH_4$ flux was strongly sensitive to the parameters of *AceProdAcemax* and *ACMinQ10*, followed by *YAceMethanogens*, *GrowRAceMethanogens*, *KAce*, and *k_dom* for all landscape types (Figure 7a), which suggested that acetate production and available C mineralization were the key controls on $CH_4$ dynamics in Arctic tundra ecosystems. Growth of methanogens also regulated $CH_4$ flux by influencing $CH_4$ production. Changes in the decomposition rate of the dissolved organic matter (DOM) had a positive influence on $CH_4$ flux for all the landscapes except the LCP rim (Figure 7a). In the high-elevation features LCP rim, HCP rim, and HCP center, the $CH_4$ flux was sensitive to the fraction of leaf nitrogen in the Rubisco enzyme functioning in photosynthesis (*flnr*). In the HCP rim, $CH_4$ dynamics also responded to changes in the decomposition rate of fungi biomass (*k_fungi*) and plant growth respiration (*grcep*; Figure 7a). Autotrophic respiration (e.g., plant growth respiration and maintenance respiration) and the *flnr* were also the key controlling factors for $CH_4$ flux in low-elevation features but exhibited opposite effects (Figure 7a).

**Table 5**
*Linear Regression Analysis for $CH_4$ Flux and Net Ecosystem Carbon Exchange (NEE) Modeled and Measured From the Eddy Covariance (EC) Tower at Daily and Hourly Time Steps*

| Variable | Time step | Estimate | Std. error | *P* value | $R^2$ |
|---|---|---|---|---|---|
| $CH_4$ flux | Daily | 0.7992 | 0.0440 | 0.0000[a] | 0.7931 |
| | Hourly | 0.7505 | 0.0204 | 0.0000[a] | 0.6135 |
| NEE | Daily | 0.7856 | 0.1242 | 0.0000[a] | 0.2943 |
| | Hourly | 1.3001 | 0.0546 | 0.0000[a] | 0.3464 |

[a]The significant level < 0.01

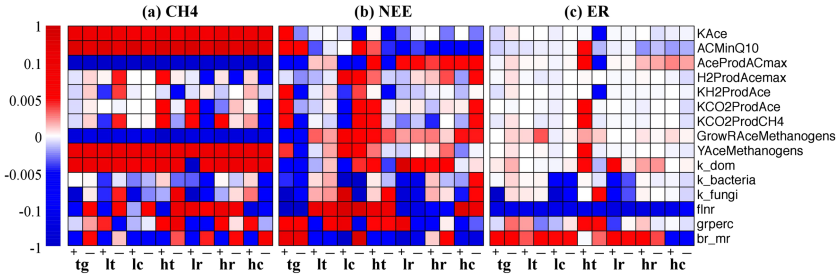


**Figure 7.** Sensitivity analysis for model response of (a) $CH_4$ fluxes, (b) net ecosystem carbon exchange (NEE), and (c) ecosystem respiration (ER) to15 parameters (*KAce, ACMinQ10, AceProdACmax, H2ProdAcemax, KH2ProdAce, KCO2ProdAce, KCO2ProdCH4, GrowRAceMethanogens, YAceMethanogens, k_dom, k_bacteria, k_fungi, flnr, grperc, and br_mr*) for trough (tg), LCP transition (lt), LCP center (lc), HCP transition (ht), LCP rim (lr), HCP rim (hr), and HCP center (hc). The symbols "+" and "-" indicate a 20% increase or 20% decrease of parameter values. Darker red and darker blue indicate a stronger positive or negative model response to parameter change. *S* is negative if the direction of model response opposes the direction of parameter change. LCP = low-centered polygon; HCP = high-centered polygon.

The most important processes of $CO_2$ dynamics are related to photosynthesis and respiration, which control $CO_2$ uptake and release across the Arctic landscape types. The *flnr* was identified as the primary factor for NEE and ER (Figure 7b and 7c). An increase in the *flnr* lead to a rise in NEE in the trough, LCP rim, and HCP rim but a NEE reduction in the LCP center, LCP transition, HCP transition, and HCP center. There was a significant decrease in ER for all landscapes with increased *flnr* (Figure 7b and 7c). For high-elevation features, including LCP rim, HCP rim, and HCP center, NEE dynamics showed negative responses to *ACMinQ10* and positive responses to *AceProdACmax*, suggesting that acetate production is also important for $CO_2$ uptake from the atmosphere (Figure 7b). In the trough, NEE was sensitive to many other parameters related to acetate production, decomposition, and respiration (Figure 7b). Beside the *flnr*, ER dynamics was sensible to maintenance respiration (*br_mr*) in both high-elevation and low-elevation landscape types (Figure 7c). Additionally, changes in the decomposition rates of bacteria and fungi biomass for the LCP center could also result in changes in ER (Figure 7c).

## 4. Discussions

### 4.1. Microtopographic Impacts on $CH_4$ and $CO_2$ Fluxes

Microtopography determines $CH_4$ and $CO_2$ dynamics in Arctic polygonal tundra by affecting the hydrological processes and thereby the soil water content, active layer depth, vegetation, and microbial functional groups in ecosystem C exchange (Davidson et al., 2016; Grant, Mekonnen, Riley, Arora, & Torn, 2017a; Lipson et al., 2012; Throckmorton et al., 2015; D. Zona et al., 2011). Soil water content was greater in the low-elevation ground of trough, LCP transition, LCP center, and HCP transition than in the high-elevation ground of the LCP rim, HCP rim, and HCP center; this discrepancy largely explained the variability in $CH_4$ fluxes among the heterogeneous landscape types in the Arctic (Grant, Mekonnen, Riley, Wainwright, et al., 2017b; Lu & Zhuang, 2012). In summer, larger $CH_4$ emissions were observed and modeled in the trough than in higher-elevation rims and centers because of the trough's higher soil water content and oversaturated soils, which is consistent with previous studies (Grant, Mekonnen, Riley, Arora, & Torn, 2017a; Schrier-Uijl et al., 2010). Saturated and oversaturated soils create an anoxic condition facilitating methanogenesis to produce $CH_4$ (von Fischer et al., 2010; Von Fischer & Hedin, 2007). Higher $CH_4$ emissions were also modeled for other low-elevation types, including LCP center, LCP transition, and HCP transition, a finding that supported the promotion effects of high soil water content on $CH_4$ production.

$CH_4$ flux is strictly produced by methanogens at very low $O_2$ concentration in soils, mainly converted from acetate and $CO_2 + H_2$ (Nazaries et al., 2013). The sensitivity analysis suggested that the substrate availability for methanogenesis resulting from acetate production and DOM decomposition was the key constraint for $CH_4$ dynamics in Arctic polygonal landscapes (Xu et al., 2015). In summer months, higher $CO_2$ uptake (i.e., lower NEE) and stronger photosynthesis (i.e., increased *flnr*) were modeled associated with the higher $CH_4$ emissions in the low-elevation ground. The results implied that a positive correlation existed between the $CO_2$ uptake and $CH_4$ emission. Stronger $CO_2$ uptake refers to a higher amount of plant biomass, which

facilitates the emission of large $CH_4$ fluxes emitting to the atmosphere via plant-mediated transport (von Fischer et al., 2010). Additionally, high $CO_2$ uptake can provide abundant C input into soils as litter for microbial decomposition, which in turn produces a high amount of available C for methanogenesis. However, the field study reported that no relationship was observed between instantaneous GPP (i.e., $CO_2$ uptake) and $CH_4$ fluxes (Davidson et al., 2016), suggesting that the processes from decomposition of organic matter to substrates for methanogenesis are very complicated and need to be considered cautiously in $CH_4$ models.

Microtopographic effects on $CO_2$ dynamics are caused primarily by changes in soil hydrological conditions and hence $O_2$ diffusion (Davidson et al., 2016; Olivas et al., 2010). Low-elevation landscape types, especially the trough and LCP center, were shown by modeling to have the largest $CO_2$ uptake in summer. Additionally, the ER via roots and microbial communities was suppressed by the low dissolved $O_2$ concentration in the saturated soils (Olivas et al., 2010; Zona et al., 2011). These results suggested that high soil moisture in Arctic tundra promotes the plant growth and suppresses the ER, eventually increasing the strength of the $CO_2$ sink in low-elevation landscapes. In contrast, lower $CO_2$ uptake and greater ER in summer were simulated for the rims and HCP center, confirming that the high-elevation ground in the Arctic acts as a smaller $CO_2$ sink (Zona et al., 2011). The ER variations in low-elevation and high-elevation landscape types in the summer months were caused largely by the difference in the availability of soil $O_2$ for microbial respiration. The strength of the $CO_2$ sink in Arctic tundra can be biased by the effects of microtopography on soil water and $O_2$ conditions. However, most landscape models have not incorporated microtopographic effects in simulating $CO_2$ fluxes. Not considering those effects might cause large biases; therefore, better simulation of microtopographic impacts is critical for model applications to C cycling in the Arctic.

### 4.2. NEE and $CH_4$ Flux at Daily and Hourly Time Steps

Biological processes occur instantaneously, on a time scale inconsistent with field measurements normally undertaken at hourly or daily scales. Ecosystem functions are more apparent at the hourly, daily, monthly, and annual scales, at which the CLM-Microbe performs. The model performance was more consistent with observed $CH_4$ and $CO_2$ fluxes for the EC domain on the daily than on the hourly scale, indicating that the model did not perform well in capturing some pulse fluxes on an hourly scale. Since the "$CH_4$ pulse" in the spring season has been widely recognized as an important component for ecosystem models in recent decades (Lu & Zhuang, 2012; Song et al., 2012; Tokida et al., 2007), an improvement of the CLM-Microbe model for better simulation of these outbreak events is needed.

In general, upscaled $CH_4$ and $CO_2$ fluxes based on modeled plot-level fluxes were able to capture most variations of measured EC fluxes at both daily and hourly time steps. We conclude that the CLM-Microbe model can be used to estimate $CO_2$ and $CH_4$ fluxes at landscape scale if fluxes are scaled by different landscape types (Schrier-Uijl et al., 2010). Moreover, the dynamics of $CH_4$ and $CO_2$ fluxes was modeled more accurately at daily than at hourly time steps. This is probably because the key factors or processes controlling $CH_4$ and $CO_2$ dynamics are slightly different across the temporal scales; but they are well defined with stable priorities in the model according to the extant knowledge, usually from observations at long time scales. Another reason for the underestimation of $CO_2$ flux might be the unexplained $CO_2$ uptake during the nongrowing season (i.e., October) in the Alaska tundra ecosystem (Figures 5b and 5d). Until confirmed mechanisms are found for the underestimation, it has no clear implications for the model performance.

### 4.3. Model Implications

This study has three implications for model development and scientific understanding of the C dynamic in the Arctic. First, the CLM-Microbe model performed well in capturing the variabilities in $CH_4$ and $CO_2$ fluxes among primary polygonal landscapes in Arctic tundra, which emphasizes the importance of spatial heterogeneity in simulating $CO_2$ and $CH_4$ fluxes in ecosystem $CH_4$ models. The model simulations indicate that the trough and transitions had estimated $CH_4$ emissions of 3.6–4.0 g $C{\cdot}m^{-2}{\cdot}year^{-1}$ annually, and the rims had a smaller annual $CH_4$ emissions of 0.7–1.1 g $C{\cdot}m^{-2}{\cdot}year^{-1}$. Differences in the annual estimates were likely due to the saturated and anoxic conditions in low-elevation ground that promote anaerobic methanogenesis, leading to a higher $CH_4$ emission. However, the annual $CH_4$ fluxes for the seven landscape types may be greatly underestimated because of the low estimates for the cold season in model simulations. Many studies have reported that >50% of annual $CH_4$ emissions occur during the cold season in Alaskan

**Table 6**
*The Comparison Between Modeled and Observed Concentrations of Belowground Dissolved Organic Carbon (DOC), $CO_2$, and $CH_4$ (g C·m$^{-3}$) Along Soil Profiles for the Trough, LCP Center and LCP Rim in 2013–2014*

| DOY | Site | Sample depth (cm) | Soil layer (CLM-microbe) | DOC | | $CO_2$ | | $CH_4$ | |
|---|---|---|---|---|---|---|---|---|---|
| | | | | Modeled | Observed | Modeled | Observed | Modeled | Observed |
| 183 | Trough | 28 | 6 | 448.11 | 282.84 | 16.08 | 156.60 | 0.55 | 0.11 |
| 240 | Trough | 22 | 5 | 478.20 | 283.92 | 0.00 | 33.00 | 0.08 | 0.14 |
| 240 | Trough | 29 | 6 | 458.43 | 222.84 | 16.15 | NA | 0.59 | NA |
| 606 | Trough | 20 | 5 | 483.29 | 118.08 | 0.00 | 48.84 | 0.01 | 0.50 |
| 606 | Trough | 37 | 6 | 462.32 | 184.80 | 16.25 | 35.16 | 0.57 | 2.06 |
| 183 | Center | 26 | 5 | 1419.74 | 30.60 | 0.00 | NA | 0.04 | NA |
| 240 | Center | 49 | 6 | 1422.88 | 1015.32 | 13.33 | NA | 0.28 | NA |
| 606 | Center | 10 | 4 | 1674.68 | 25.68 | 0.00 | NA | 0.02 | NA |
| 183 | Rim | 29 | 6 | 1064.58 | NA | 4.13 | NA | 0.09 | NA |
| 183 | Rim | 7 | 3 | 1120.60 | 29.16 | 618.30 | NA | 0.05 | NA |
| 240 | Rim | 7 | 3 | 1178.37 | 30.72 | 618.34 | NA | 0.14 | NA |
| 240 | Rim | 37 | 6 | 1073.85 | 66.72 | 4.20 | NA | 0.20 | NA |

tundra (September to May; Kittler et al., 2017; Zona et al., 2016). Moreover, our estimate of annual $CH_4$ fluxes for the entire study area was smaller compared with similar studies in Arctic tundra (Reeburgh et al., 1998; Wille et al., 2008). This discrepancy might be explained by the lower organic matter density or less plant cover in our study area. For example, the less abundant plant cover reduces the plant-mediated transport of $CH_4$ and therefore lowers $CH_4$ emissions (Bhullar et al., 2013). The variations in our estimates for seven landscape types were potentially biased because they ignored the lateral surface hydrologic and thermal processes. The spatial variability in soil moisture and soil temperature can be overpredicted if the lateral subsurface hydrologic and thermal processes are excluded (Bisht et al., 2018), and the same is true for the spatial variability in $CH_4$ emissions in Arctic polygonal landscapes. By incorporating these surface processes, the $CH_4$ models can improve the representation of lateral hydrologic and thermal transport, and thereby improve the accuracy of estimations (Aas et al., 2019).

Second, the potential shifts in Arctic tundra ecosystems as C sinks or sources is valuable information for climate projections. This study showed that the trough is the only net $CO_2$ sink among all landscape types and plays a key role in ecosystem C storage because of its 35% areal share of the entire study area. $CO_2$ dynamics in the trough were very sensitive to many processes related to photosynthesis, plant and soil respiration, and C mineralization and distribution. It is possible for trough shifting to being net C sources from net C sinks, even with a tiny change in $CO_2$ processes under climate changes. Annual estimates indicated that the HCPs were 310% greater $CO_2$ sources than the LCPs. Additionally, greater ER was estimated in the HCPs than in the LCPs. The HCP center, in particular, had an ER of 928.0 g C·m$^{-2}$, the highest among the landscape types. Because LCPs may eventually subside into HCPs, $CO_2$ emissions from Arctic soils tend to increase rapidly not only because of the effects of climate changes but also because of the changes in landscape patterns.

Finally, this study advocates the mechanistic modeling of C cycling to better estimate $CO_2$ and $CH_4$ fluxes across the Arctic tundra ecosystems. It is well known that differences in $CH_4$ and $CO_2$ emissions across the Arctic landscapes are directly led by the mechanisms and dynamics of microbial activities in relation to C mineralization, decomposition, respiration, methanogenesis, and methanotrophy. By including these microbial processes, the CLM-Microbe model allows us to understand the mechanisms of Arctic C cycling according to the production and consumption processes of $CO_2$ and $CH_4$. Soil DOC, $CH_4$, and $CO_2$ concentrations were modeled and compared with the measured concentrations for the landscape types and soil depths for a few data points (Table 6). Modeled DOC concentrations were ~1.6 times the measurements at the middle layer of soils in the trough on day of year (DOY) 183 and DOY 240 of 2013; these results suggested that the model could be useful for simulating the concentrations of C compounds. In Arctic ecosystems, high $CH_4$ emissions in saturated soils were modeled with high $CH_4$ production, which was consistent with the large amount of modeled acetoclastic methanogens. $CH_4$ oxidation was strengthened by high $O_2$ availability in the topsoil of the rims and HCP center compared with saturated trough and transitions. Moreover, differences in $CH_4$ transport via diffusion, ebullition, and plant-mediated transport were modeled with seasonal

variations. Large $CH_4$ fluxes emitted from soils were associated with the fast plant growth in summer. Furthermore, soil microbial structure and biomass were simulated to understand the $CO_2$ and $CH_4$ dynamics, which suggested the importance of belowground microbial mechanisms in modeling surface $CO_2$ and $CH_4$ fluxes.

### 4.4. The Way Forward

The CLM-Microbe model can simulate the belowground microbial processes for surface $CO_2$ and $CH_4$ fluxes. Although promising results proved the robustness of the CLM-Microbe model in simulating surface $CO_2$ and $CH_4$ fluxes, a number of tasks were identified as follow-up efforts to this study. First, although the upscaling results with an area-weighted approach seems promising, the dominant roles of landscape types weakened the variations in C flux. Upscaling with a mechanistic model should provide more accurate quantification of the C flux on a regional scale, as well as a finer-resolution C flux at both the spatial and the temporal scales (Watts et al., 2014). Second, belowground C dynamics—for example, DOC, acetate, $CO_2$, and $CH_4$ concentrations—are important variables and precursors for observed surface gas fluxes. We call for a data-model integration approach to better integrate the observational data and better simulate belowground processes and surface flux. Third, hydrological dynamics is the key control for biogeochemical processes, particularly for the changing Arctic. Improving the model's ability to simulate hydrology is an important cornerstone for simulating soil biogeochemistry. Fourth, microbial genomic information is the most accurate information for microbial functions, yet it has not been well utilized for model parameterization. The CLM-Microbe model is capable of simulating the relative abundance of methanogenesis; thus, it is worthwhile to improve the model to better simulate the microbial functional groups responsible for $CH_4$ production and consumption. Fifth, although C flux data, particularly the $CH_4$ flux, have been scarce across the Arctic tundra ecosystem, recent projects and technical improvements have allowed year-round measurements. Those data can serve as a good constraint for the CLM-Microbe model at multiple scales; a multiscale "MODEX" (model-observation-experiment) framework to better integrate multiple observational data to quantify gas flux and understand its mechanisms in the Arctic is much needed.

## 5. Conclusions

This study reported the application of the CLM-Microbe model to seven microtopographic landscape types in the Arctic tundra near Utqiagvik, AK. The model results were promising and consistent with the observational gas fluxes. The modeled results showed that low-elevation landscape types (e.g. trough, transitions, and LCP center) have higher $CH_4$ emission with greater seasonal variations than high-elevation landscape types (e.g. rims and HCP center), as a result of the greater soil saturation in the low-elevation landscape types. Model sensitivity analysis determined that the substrate (e.g. acetate, $CO_2$ + $H_2$) availability for methanogens was the most important factor in controlling $CH_4$ emissions in Arctic ecosystems, and plant photosynthesis greatly affected the NEE and ER. The model performed more accurately in simulating the daily EC fluxes than hourly fluxes, indicating the importance of the time scale in simulating gas fluxes.

The large spatial heterogeneity in $CO_2$ and $CH_4$ fluxes across the Arctic landscape requires explicit consideration and modeling of microtopography, as well as of the mechanisms controlling C biogeochemistry in response to hydrology dynamics. As the climate continues to warm rapidly in the Arctic, large variations at both the spatial and the temporal scales are anticipated across the Arctic landscape. Dramatic changes in land surface $CO_2$ and $CH_4$ fluxes might alter the land–atmosphere feedback in the Arctic. An insightful regional-scale investigation of the thermal conditions, hydrology, and biogeochemistry across the pan-Arctic is urgently needed and will benefit the entire scientific community and the public.

**Acknowledgments**
We are grateful to Randy A. Dahlgren from University of California, Davis for his constructive suggestions for results interpretation. The authors are grateful for financial and facility support from San Diego State University. Financial assistance was partially provided by the SPRUCE and NGEE Arctic projects, which are supported by the Office of Biological and Environmental Research in the Department of Energy Office of Science. This project is partially supported by the U.S. National Science Foundation (1702797).

## Data Availability Statement

The data used in this study have been archived at the NGEE-Arctic data repository, including gas flux data (DOI: 10.5440/1362279), and meteorological data (https://ngee-arctic.ornl.gov/data/).

## References

Aas, K. S., Martin, L., Nitzbon, J., Langer, M., Boike, J., Lee, H., et al. (2019). Thaw processes in ice-rich permafrost landscapes represented with laterally coupled tiles in a land surface model. *The Cryosphere*, *13*(2), 591–609. https://doi.org/10.5194/tc-13-591-2019

Abolt, C. J., Young, M. H., Atchley, A. L., & Harp, D. R. (2018). Microtopographic control on the ground thermal regime in ice wedge polygons. *The Cryosphere*, *12*(6), 1957–1968. https://doi.org/10.5194/tc-12-1957-2018

Atchley, A. L., Coon, E. T., Painter, S. L., Harp, D. R., & Wilson, C. J. (2016). Influences and interactions of inundation, peat, and snow on active layer thickness. *Geophysical Research Letters*, *43*, 5116–5123. https://doi.org/10.1002/2016gl068550

Belshe, E. F., Schuur, E. A. G., & Bolker, B. M. (2013). Tundra ecosystems observed to be $CO_2$ sources due to differential amplification of the carbon cycle. *Ecology Letters*, *16*(10), 1307–1315. https://doi.org/10.1111/ele.12164

Bhullar, G. S., Edwards, P. J., & Olde Venterink, H. (2013). Variation in the plant-mediated methane transport and its importance for methane emission from intact wetland peat mesocosms. *Journal of Plant Ecology*, *6*(4), 298–304. https://doi.org/10.1093/jpe/rts045

Bisht, G., Riley, W. J., Wainwright, H. M., Dafflon, B., Yuan, F., & Romanovsky, V. E. (2018). Impacts of microtopographic snow redistribution and lateral subsurface processes on hydrologic and thermal states in an Arctic polygonal ground ecosystem: A case study using ELM-3D v1. 0. *Geoscientific Model Development*, *11*(1). https://doi.org/10.5194/gmd-11-61-2018

Bridgham, S. D., Cadillo-Quiroz, H., Keller, J. K., & Zhuang, Q. (2013). Methane emissions from wetlands: Biogeochemical, microbial, and modeling perspectives from local to global scales. *Global Change Biology*, *19*(5), 1325–1346. https://doi.org/10.1111/gcb.12131

Davidson, S. J., Sloan, V. L., Phoenix, G. K., Wagner, R., Fisher, J. P., Oechel, W. C., & Zona, D. (2016). Vegetation type dominates the spatial variability in $CH_4$ emissions across multiple Arctic tundra landscapes. *Ecosystems*, *19*(6), 1116–1132. https://doi.org/10.1007/s10021-016-9991-0

Ebrahimi, A., & Or, D. (2017). Mechanistic modeling of microbial interactions at pore to profile scale resolve methane emission dynamics from permafrost soil. *Journal of Geophysical Research: Biogeosciences*, *122*, 1216–1238. https://doi.org/10.1002/2016jg003674

Gilks, W. R., Richardson, S., & Spiegelhalter, D. J. (1998). *Markov chain Monte Carlo in practice*, (Vol. xvii, p. 486). Boca RatonFla.: Chapman & Hall. https://doi.org/10.1201/b14835

Grant, R. F. (1998). Simulation of methanogenesis in the mathematical model *ecosys*. *Soil Biology and Biochemistry*, *30*, 883–896. https://doi.org/10.1016/S0038-0717(97)00218-6

Grant, R. F., Mekonnen, Z. A., Riley, W. J., Arora, B., & Torn, M. S. (2017a). Mathematical modelling of Arctic polygonal tundra with Ecosys: 2. Microtopography determines how $CO_2$ and $CH_4$ exchange responds to changes in temperature and precipitation. *Journal of Geophysical Research: Biogeosciences*, *122*, 3174–3187. https://doi.org/10.1002/2017jg004037

Grant, R. F., Mekonnen, Z. A., Riley, W. J., Wainwright, H. M., Graham, D., & Torn, M. S. (2017b). Mathematical modelling of Arctic polygonal tundra with Ecosys: 1. Microtopography determines how active layer depths respond to changes in temperature and precipitation. *Journal of Geophysical Research: Biogeosciences*, *122*, 3161–3173. https://doi.org/10.1002/2017jg004035

Herndon, E. M., Mann, B. F., Roy Chowdhury, T., Yang, Z., Wullschleger, S. D., Graham, D., et al. (2015a). Pathways of anaerobic organic matter decomposition in tundra soils from Barrow, Alaska. *Journal of Geophysical Research: Biogeosciences*, *120*, 2345–2359. https://doi.org/10.1002/2015JG003147

Herndon, E. M., Yang, Z., Bargar, J., Janot, N., Regier, T. Z., Graham, D. E., et al. (2015). Geochemical drivers of organic matter decomposition in Arctic tundra soils. *Biogeochemistry*, *126*(3), 397–414. https://doi.org/10.1007/s10533-015-0165-5

Hinkel, K. M., Frohn, R. C., Nelson, F. E., Eisner, W. R., & Beck, R. A. (2005). Morphometric and spatial analysis of thaw lakes and drained thaw lake basins in the western Arctic coastal plain, Alaska. *Permafrost and Periglacial Processes*, *16*(4), 327–341. https://doi.org/10.1002/ppp.532

Jørgensen, C. J., Lund Johansen, K. M., Westergaard-Nielsen, A., & Elberling, B. (2014). Net regional methane sink in high Arctic soils of Northeast Greenland. *Nature Geoscience*, *8*(1), 20–23. https://doi.org/10.1038/ngeo2305

Kaiser, S., Göckede, M., Castro-Morales, K., Knoblauch, C., Ekici, A., Kleinen, T., et al. (2017). Process-based modelling of the methane balance in periglacial landscapes (JSBACH-methane). *Geoscientific Model Development*, *10*(1), 333–358. https://doi.org/10.5194/gmd-10-333-2017

Kettunen, A. (2003). Connecting methane fluxes to vegetation cover and water table fluctuations at microsite level: A modeling study. *Global Biogeochemical Cycles*, *17*(2), 1051. https://doi.org/10.1029/2002GB001958

Kittler, F., Heimann, M., Kolle, O., Zimov, N., Zimov, S., & Göckede, M. (2017). Long-term drainage reduces $CO_2$ uptake and $CH_4$ emissions in a Siberian permafrost ecosystem. *Global Biogeochemical Cycles*, *31*, 1704–1717. https://doi.org/10.1002/2017gb005774

Koven, C. D., Riley, W., Subin, Z. M., Tang, J., Torn, M. S., Collins, W. D., et al. (2013). The effect of vertically-resolved soil biogeochemistry and alternate soil C and N models on C dynamics of CLM4. *Biogeosciences*, *10*, 7109–7131. https://doi.org/10.5194/bg-10-7109-2013

Kumar, J., Collier, N., Bisht, G., Mills, R. T., Thornton, P. E., Iversen, C. M., & Romanovsky, V. (2016). Modeling the spatiotemporal variability in subsurface thermal regimes across a low-relief polygonal tundra landscape. *The Cryosphere*, *10*, 2241–2274. https://doi.org/10.5194/tc-10-2241-2016

Langford, Z., Kumar, J., Hoffman, F., Norby, R., Wullschleger, S., Sloan, V., & Iversen, C. (2016). Mapping arctic plant functional type distributions in the barrow environmental observatory using WorldView-2 and LiDAR datasets. *Remote Sensing*, *8*, 733. https://doi.org/10.3390/rs8090733

Liljedahl, A. K., Hinzman, L. D., Harazono, Y., Zona, D., Tweedie, C. E., Hollister, R. D., et al. (2011). Nonlinear controls on evapotranspiration in arctic coastal wetlands. *Biogeosciences*, *8*(11), 3375–3389. https://doi.org/10.5194/bg-8-3375-2011

Lipson, D. A., Raab, T. K., Goria, D., & Zlamal, J. (2013). The contribution of Fe (III) and humic acid reduction to ecosystem respiration in drained thaw lake basins of the Arctic coastal plain. *Global Biogeochemical Cycles*, *27*, 399–409. https://doi.org/10.1002/gbc.20038

Lipson, D. A., Zona, D., Raab, T. K., Bozzolo, F., Mauritz, M., & Oechel, W. C. (2012). Water table height and microtopography control biogeochemical cycling in an Arctic coastal tundra ecosystem. *Biogeosciences*, *9*, 577–591. https://doi.org/10.1002/gbc.20038

Lu, X. L., & Zhuang, Q. L. (2012). Modeling methane emissions from the Alaskan Yukon River basin, 1986–2005, by coupling a large-scale hydrological model and a process-based methane model. *Journal of Geophysical Research – Biogeosciences*, *117*, G02010. https://doi.org/10.1029/2011jg001843

Nauta, A. L., Heijmans, M. M., Blok, D., Limpens, J., Elberling, B., Gallagher, A., et al. (2015). Permafrost collapse after shrub removal shifts tundra ecosystem to a methane source. *Nature Climate Change*, *5*, 67–70. https://doi.org/10.1038/nclimate2446

Nazaries, L., Murrell, J. C., Millard, P., Baggs, L., & Singh, B. K. (2013). Methane, microbes and models: Fundamental understanding of the soil methane cycle for future predictions. *Environmental Microbiology*, *15*, 2395–2417. https://doi.org/10.1111/1462-2920.12149

Newman, B. D., Throckmorton, H. M., Graham, D. E., Gu, B., Hubbard, S. S., Liang, L., et al. (2015). Microtopographic and depth controls on active layer chemistry in Arctic polygonal ground. *Geophysical Research Letters*, *42*, 1808–1817. https://doi.org/10.1002/2014gl062804

Oechel, W. C., Hastings, S. J., Vourlitis, G., Jenkins, M., Riechers, G., & Grulke, N. (1993). Recent change of Arctic tundra ecosystems from a net carbon-dioxide sink to a source. *Nature*, *361*, 520–523. https://doi.org/10.1038/361520a0

Oh, Y., Stackhouse, B., Lau, M. C. Y., Xu, X., Trugman, A. T., Moch, J., et al. (2016). A scalable model for methane consumption in arctic mineral soils. *Geophysical Research Letters*, *43*, 5143–5150. https://doi.org/10.1002/2016gl069049

Olivas, P. C., Oberbauer, S. F., Tweedie, C. E., Oechel, W. C., & Kuchy, A. (2010). Responses of $CO_2$ flux components of Alaskan coastal plain tundra to shifts in water table. *Journal of Geophysical Research – Biogeosciences*, *115*, G00I05. https://doi.org/10.1029/2009jg001254

Raz-Yaseef, N. Billesbach, D., Torn M. (2013). Eddy-covariance and auxiliary measurements, NGEE-Barrow, 2012-2013. Next generation ecosystem experiments Arctic data collection, oak Ridge National Laboratory, U.S. Department of Energy, oak ridge, Tennessee, USA. Dataset accessed on July 1st 2015 at https://doi.org/10.5440/1362279.

Reeburgh, W. S., King, J. Y., Regli, S. K., Kling, G. W., Auerbach, N. A., & Walker, D. A. (1998). A $CH_4$ emission estimate for the Kuparuk River basin, Alaska. *Journal of Geophysical Research-Atmospheres*, *103*, 29,005–29,013. https://doi.org/10.1029/98jd00993

Riley, W. J., Subin, Z. M., Lawrence, D. M., Swenson, S. C., Torn, M. S., Meng, L., et al. (2011). Barriers to predicting changes in global terrestrial methane fluxes: Analyses using CLM4Me, a methane biogeochemistry model integrated in CESM. *Biogeosciences*, *8*, 1925–1953. https://doi.org/10.5194/bg-8-1925-2011

Schrier-Uijl, A. P., Kroon, P. S., Hensen, A., Leffelaar, P. A., Berendse, F., & Veenendaal, E. M. (2010). Comparison of chamber and eddy covariance-based $CO_2$ and $CH_4$ emission estimates in a heterogeneous grass ecosystem on peat. *Agricultural and Forest Meteorology*, *150*, 825–831. https://doi.org/10.1016/j.agrformet.2009.11.007

Segers, R., & Kengen, S. W. M. (1998). Methane production as a function of anaerobic carbon mineralization: A process model. *Soil Biology and Biochemistry*, *30*, 1107–1117. https://doi.org/10.1016/S0038-0717(97)00198-3

Semenchuk, P. R., Elberling, B., Amtorp, C., Winkler, J., Rumpf, S., Michelsen, A., & Cooper, E. J. (2015). Deeper snow alters soil nutrient availability and leaf nutrient status in high Arctic tundra. *Biogeochemistry*, *124*, 81–94. https://doi.org/10.1007/s10533-015-0082-7

Song, C., Xu, X., Sun, X., Tian, H., Sun, L., Miao, Y., et al. (2012). Large methane emission upon spring thaw from natural wetlands in the northern permafrost region. *Environmental Research Letters*, *7*, 34009. https://doi.org/10.1088/1748-9326/7/3/034009

Sturtevant, C. S., & Oechel, W. C. (2013). Spatial variation in landscape-level $CO_2$ and $CH_4$ fluxes from arctic coastal tundra: Influence from vegetation, wetness, and the thaw lake cycle. *Global Change Biology*, *19*(9), 2853–2866. https://doi.org/10.1111/gcb.12247

Tan, Z., Zhuang, Q., Henze, D. K., Frankenberg, C., Dlugokencky, E., Sweeney, C., & Turner, A. J. (2015). Mapping pan-Arctic methane emissions at high spatial resolution using an adjoint atmospheric transport and inversion method and process-based wetland and lake biogeochemical models. *Atmospheric Chemistry and Physics Discussions*, *15*, 32,469–32,518. https://doi.org/10.5194/acpd-15-32469-2015

Tas, N., Prestat, E., Wang, S., Wu, Y., Ulrich, C., Kneafsey, T., et al. (2018). Landscape topography structures the soil microbiome in arctic polygonal tundra. *Nature Communications*, *9*(1), 777. https://doi.org/10.1038/s41467-018-03089-z

Thauer, R. K., Kaster, A.-K., Seedorf, H., Buckel, W., & Hedderich, R. (2008). Methanogenic archaea: Ecologically relevant differences in energy conservation. *Nature Reviews Microbiology*, *6*(8), 579–591. https://doi.org/10.1038/nrmicro1931

Thauer, R. K., Zinkhan, D., & Spormann, A. (1989). Biochemistry of acetate catabolism in anaerobic chemotrophic bacteria. *Annual Reviews in Microbiology*, *43*, 43–67. https://doi.org/10.1146/annurev.mi.43.100189.000355

Thornton, P. E., Lamarque, J.-F., Rosenbloom, N. A., & Mahowald, N. M. (2007). Influence of carbon-nitrogen cycle coupling on land model response to $CO_2$ fertilization and climate variability. *Global Biogeochemical Cycles*, *21*, GB4018. https://doi.org/10.1029/2006gb002868

Thornton, P. E., & Rosenbloom, N. A. (2005). Ecosystem model spin-up: Estimating steady state conditions in a coupled terrestrial carbon and nitrogen cycle model. *Ecological Modelling*, *189*, 25–48. https://doi.org/10.1016/j.ecolmodel.2005.04.008

Throckmorton, H. M., Heikoop, J. M., Newman, B. D., Altmann, G. L., Conrad, M. S., Muss, J. D., & Wilson, C. J. (2015). Pathways and transformations of dissolved methane and dissolved inorganic carbon in Arctic tundra watersheds: Evidence from analysis of stable isotopes. *Global Biogeochemical Cycles*, *29*, 1893–1910. https://doi.org/10.1002/2014GB005044

Tian, H., Xu, X., Liu, M., Ren, W., Zhang, C., Chen, G., & Lu, C. (2010). Spatial and temporal patterns of $CH_4$ and $N_2O$ fluxes in terrestrial ecosystems of North America during 1979-2008: Application of a global biogeochemistry model. *Biogeosciences*, *7*, 2673–2694. https://doi.org/10.5194/bg-7-2673-2010

Tokida, T., Mizoguchi, M., Miyazaki, T., Kagemoto, A., Nagata, O., & Hatano, R. (2007). Episodic release of methane bubbles from peatland during spring thaw. *Chemosphere*, *70*(2), 165–171. https://doi.org/10.1016/j.chemosphere.2007.06.042

Torn, M. S. (2016). CO2 CH4 flux air temperature soil temperature and soil moisture, Barrow, Alaska 2013 ver. 1. Retrieved from: http://ngee-arctic.ornl.gov/

Von Fischer, J. C., & Hedin, L. O. (2007). Controls on soil methane fluxes: Tests of biophysical mechanisms using stable isotope tracers. *Global Biogeochemical Cycles*, *21*, GB2007. https://doi.org/10.1029/2006GB002687

von Fischer, J. C., Rhew, R. C., Ames, G. M., Fosdick, B. K., & von Fischer, P. E. (2010). Vegetation height and other controls of spatial variability in methane emissions from the Arctic coastal tundra at Barrow, Alaska. *Journal of Geophysical Research, Biogeosciences (2005–2012)*, *115*, G00I03. https://doi.org/10.1029/2009JG001283

Wagner, R., Zona, D., Oechel, W., & Lipson, D. (2017). Microbial community structure and soil pH correspond to methane production in Arctic Alaska soils. *Environmental Microbiology*, *19*, 3398–3410. https://doi.org/10.1111/1462-2920.13854

Wainwright, H. M., Liljedahl, A. K., Dafflon, B., Ulrich, C., Peterson, J. E., Gusmeroli, A., & Hubbard, S. S. (2017). Mapping snow depth within a tundra ecosystem using multiscale observations and Bayesian methods. *The Cryosphere*, *11*(2), 857–875. https://doi.org/10.5194/tc-11-857-2017

Walter, B. P., & Heimann, M. (2000). A process-based, climate-sensitive model to derive methane emissions from natural wetlands: Application to five wetland sites, sensitivity to model parameters, and climate. *Global Biogeochemical Cycles*, *14*, 745–765. https://doi.org/10.1029/1999GB001204

Wania, R., Ross, I., & Prentice, I. C. (2010). Implementation and evaluation of a new methane model within a dynamic global vegetation model: LPJ-WHyMe v1.3.1. *Geoscientific Model Development*, *3*, 565–584. https://doi.org/10.5194/gmd-3-565-2010

Watts, J. D., Kimball, J. S., Parmentier, F. J. W., Sachs, T., Rinne, J., Zona, D., et al. (2014). A satellite data driven biophysical modeling approach for estimating northern peatland and tundra $CO_2$ and $CH_4$ fluxes. *Biogeosciences*, *11*, 1961–1980. https://doi.org/10.5194/bg-11-1961-2014

Wille, C., Kutzbach, L., Sachs, T., Wagner, D., & Pfeiffer, E.-M. (2008). Methane emission from Siberian arctic polygonal tundra: Eddy covariance measurements and modeling. *Global Change Biology*, *14*, 1395–1408. https://doi.org/10.1111/j.1365-2486.2008.01586.x

Xu, X., & Yuan, F. (2016). *Meteorological forcing at Barrow AK 1981–2013*. Retrieved from http://ngee-arctic.ornl.gov/

Xu, X., Yuan, F., Hanson, P. J., Wullschleger, S. D., Thornton, P. E., Riley, W. J., et al. (2016). Review and synthesis: Four decades of modeling methane cycling within terrestrial ecosystems. *Biogeosciences*, *13*, 3735–3755. https://doi.org/10.5194/bg-13-3735-2016

Xu, X. F., Elias, D. A., Graham, D. E., Phelps, T. J., Carrol, S. L., Wullschleger, S. D., & Thornton, P. E. (2015). A microbial functional group based module for simulating methane production and consumption: Application to an incubation permafrost soil. *Journal of Geophysical Research: Biogeosciences*, *120*, 1315–1333. https://doi.org/10.1002/2015JG002935

Xu, X. F, Hahn, M. S., Kumar, J., Yuan, F., Tang, G., Thornton, P., et al. (2014), Upscaling Plot-Scale Methane Flux to a Eddy Covariance Tower Domain in Barrow, AK: Integrating in-situ data with a microbial functional group-based model, paper presented at AGU Fall Meeting Abstracts.

Xu, X. F., Tian, H. Q., Zhang, C., Liu, M. L., Ren, W., Chen, G. S., et al. (2010). Attribution of spatial and temporal variations in terrestrial methane flux over North America. *Biogeosciences*, *7*, 3637–3655. https://doi.org/10.5194/bg-7-3637-2010

Yuan, F., Wang, G., Painter, S. L., Tang, G., Xu, X., Kumar, J., et al. (2017). *Effect of Freeze-Thaw Cycles on Soil Nitrogen Reactive Transport in a Polygonal Arctic Tundra Ecosystem at Barrow AK Using 3-D Coupled ALM-PFLOTRAN*. In AGU Fall Meeting Abstracts.

Zhang, Y., Sachs, T., Li, C., & Boike, J. (2012). Upscaling methane fluxes from closed chambers to eddy covariance based on a permafrost biogeochemistry integrated model. *Global Change Biology*, *18*, 1428–1440. https://doi.org/10.1111/j.1365-2486.2011.02587.x

Zhuang, Q., Melillo, J. M., Kicklighter, D. W., Prinn, R. G., McGuire, A. D., Steudler, P. A., et al. (2004). Methane fluxes between terrestrial ecosystems and the atmosphere at northern high latitudes during the past century: A retrospective analysis with a process-based biogeochemistry model. *Global Biogeochemical Cycles*, *18*, GB3010. https://doi.org/10.1029/2004GB002239

Zona, D., Gioli, B., Commane, R., Lindaas, J., Wofsy, S. C., Miller, C. E., et al. (2016). Cold season emissions dominate the Arctic tundra methane budget. *Proceedings of the National Academy of Sciences*, *113*(1), 40–45. https://doi.org/10.1073/pnas.1516017113

Zona, D., Lipson, D. A., Zulueta, R. C., Oberbauer, S. F., & Oechel, W. C. (2011). Microtopographic controls on ecosystem functioning in the Arctic coastal plain. *Journal of Geophysical Research – Biogeosciences*, *116*, G00I08. https://doi.org/10.1029/2009jg001241